Electronic Supplementary Material (ESI) for Soft Matter

Contact-controlled amoeboid motility induces dynamic cell trapping in 3D-microstructured surfaces

Delphine Arcizet[◊¤], Sofia Capito[◊], Mari Gorelashvili, Carolin Leonhardt, Marion Vollmer, Simon Youssef Susanne Rappl, and Doris Heinrich[*]

Center for Nanoscience (CeNS) and Faculty of Physics, Ludwig-Maximilians-Universität München, Geschwister-Scholl-Platz 1, 80539 München, Germany

[*] To whom correspondence should be addressed; E-mail: doris.heinrich@lmu.de
[◊] These two authors contributed equally to this work.
[¤] Current address: Institut de Biologie Structurale Jean-Pierre Ebel, Commissariat à l'Energie Atomique, 41 rue Jules Horowitz, 38027 Grenoble

MULTIMEDIA FILES AND SUPPORTING INFORMATION

This file contains:

A. Supplementary Figures and Tables

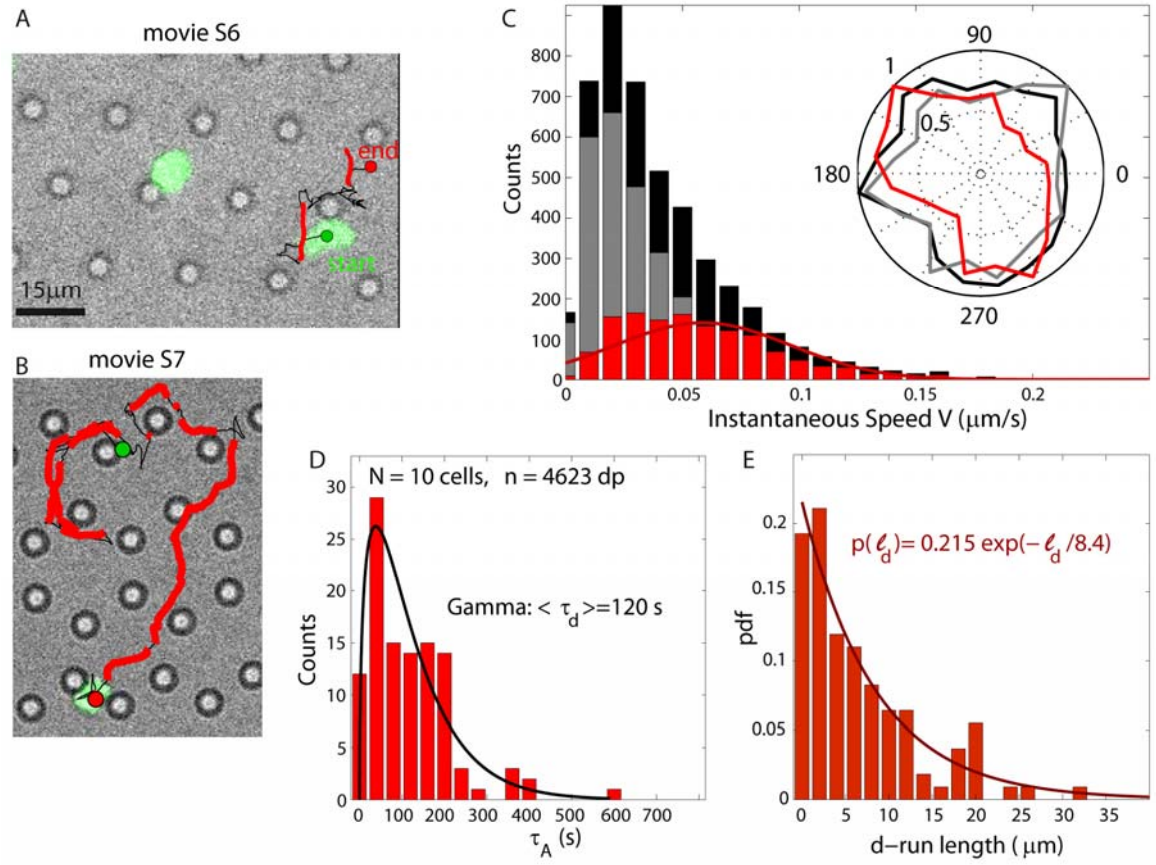

Figure S1: *D. discoideum* migration within pillar fields of high interpillar distance ($>15\mu m$).
(A – movie S6, B – movie S7) Typical cell migration tracks, displaying *dir*-runs from pillar to pillar: the cell (green) is efficiently guided from pillar to pillar, and covers a very long distance (B).
(C-E) Statistics on 10 measured cells. (C) The speed distribution is shifted towards lower values compared to flat, and the angle distribution remains random for *dir*- and *rm*-modes (insert). (D) The *dir*-run lifetimes are fitted by a Gamma distribution of average value 120 s, 22% smaller than on flat. (E) The distribution of distances covered during *dir*-runs is fitted by an exponential decay of typical cut-off length 8.4µm.

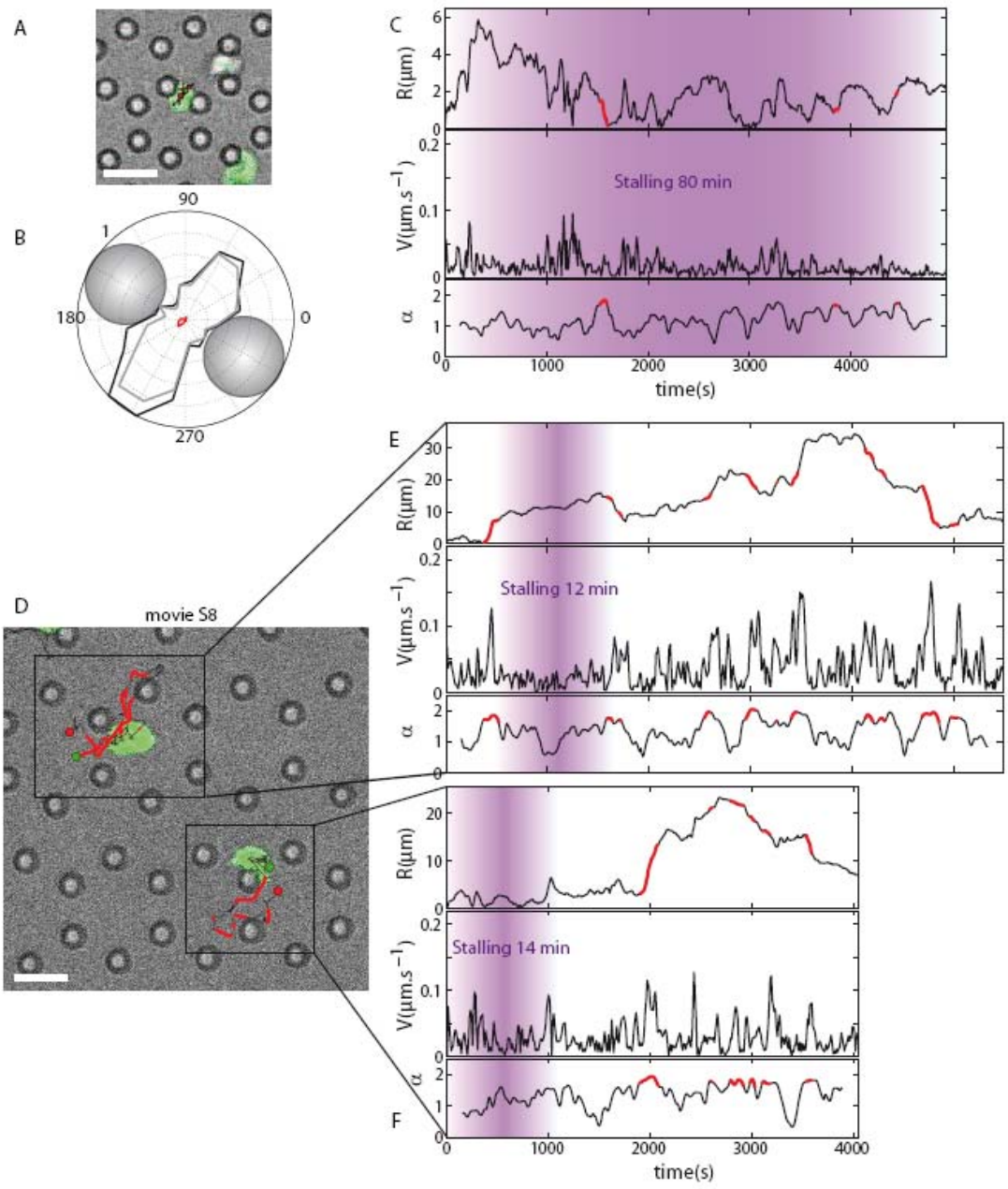

Figure S2: *D. discoideum* cells stalling within a pillar field where the interpillar distance equals the cell diameter.
(A-C) A cell is stalled between two pillars, during the whole recording time of over 80 min (A). The angle distribution shows back and forth oscillations between pillars without any net motion (B). The time series reveals a strong decrease in cell velocity (C). (D-F- movie S8) Two cells are stalled for a certain fraction of their recorded trajectory, as evidenced through their tracks (D), and time series (E, F).

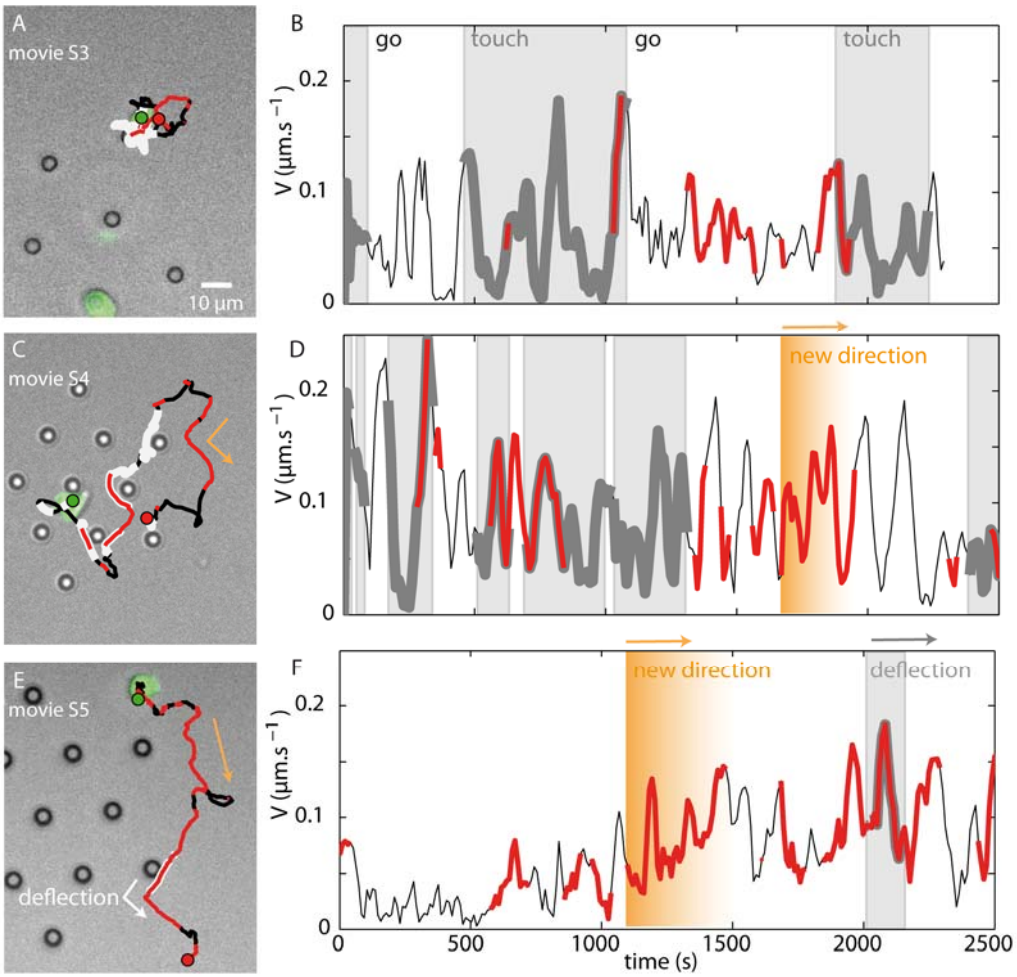

Figure S3: Modification of spontaneous migration upon contact with micron-scaled surface features.
Various scenarios of cell-pillar interactions: micrographs with individual cell tracks (A, C, E, with "touch" phases in white, *dir*-runs in red) and time sequences of the instantaneous cell speed *V* (B, D, F, "touch" phases in light gray).
(A, B) Revisiting track: the cell goes back and forth to the same pillar in an *rm*-type of motion for 40 min. Very rare *dir*-runs are present when the cell tries to escape from the pillar, and the cell is essentially trapped around the pillar.
(C, D) Guided track: the cell is guided from pillar to pillar within an island of microstructures, exhibiting a "stick-and-go" type of motion: after displaying several sequences of touching (grey) and going, the cell leaves the island, probes its surrounding flat environment, and finally repolarizes into a new direction (orange) until it finds a pillar again.
(E, F) Deflecting track: the cell probes its surrounding flat environment, polarizes into a certain direction (orange shading), increasing its speed (red arrow). After a new probing and re-polarizing event, V increases again (red arrow) and upon the next pillar contact, the cell is simply deflected by the pillar.

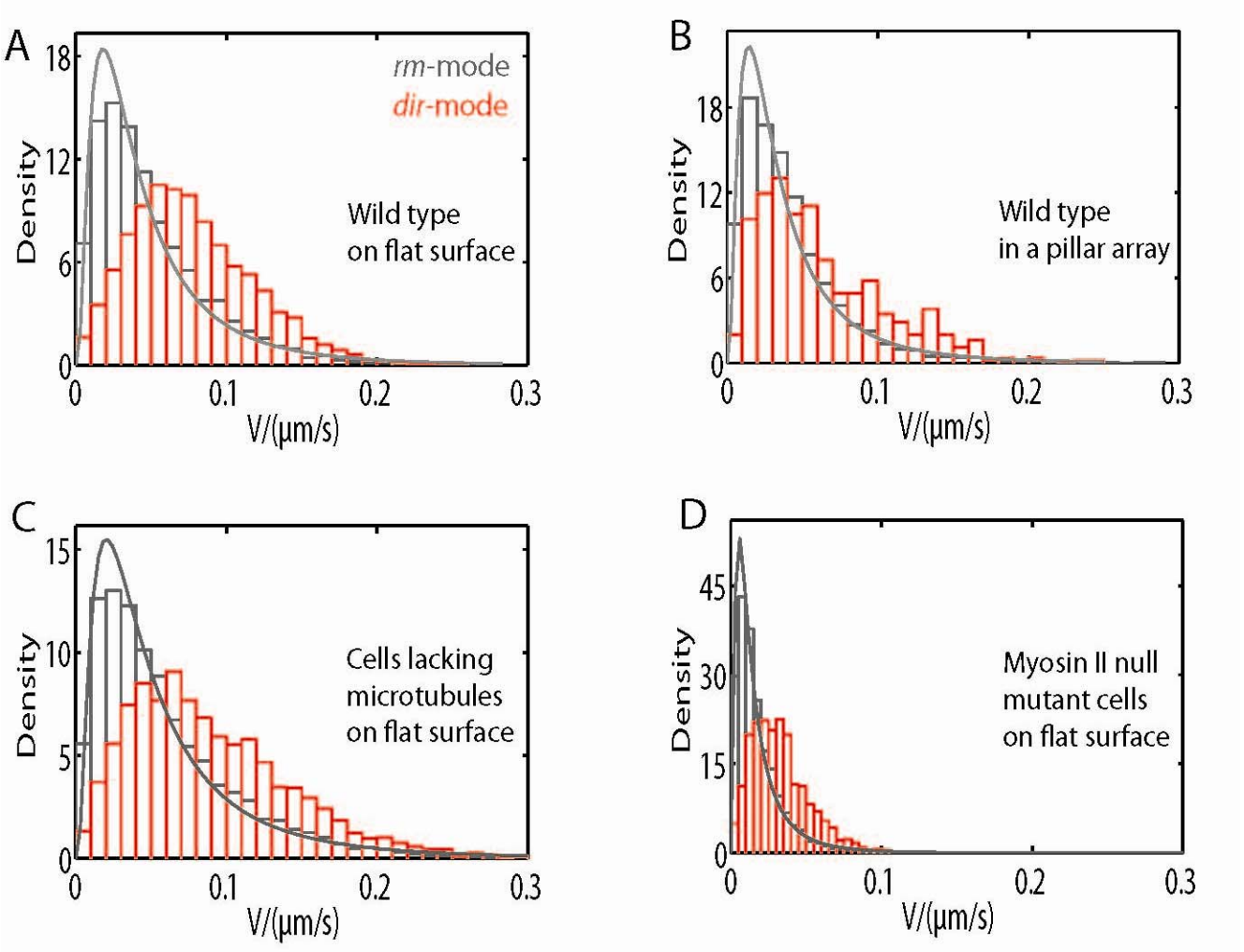

Figure S4: Quantitative Analysis of Velocity Distributions

(A) Instantaneous speed distributions, resulting from all analyzed wild-type cells on flat PDMS (red: *d*-runs, grey: *rm*-modes). The speed distribution of *rm*-modes is best fitted by a log-normal curve. (B) Instantaneous speed distributions, resulting from all analyzed wild-type cells within a micropillar array (red: *d*-runs, grey: *rm*-modes). The speed distribution of *rm*-modes is best fitted by a log-normal curve. (C) Instantaneous speed distributions, resulting from all analyzed cells lacking microtubules within a micropillar array (red: *d*-runs, grey: *rm*-modes). The speed distribution of *rm*-modes is best fitted by a log-normal curve. (D) Instantaneous speed distributions, resulting from all analyzed Myosin II null cells within micropillar array (red: *d*-runs, grey: *rm*-modes). The speed distribution of *rm*-modes is best fitted by a log-normal curve.

Micropillar array : interpillar distance		**<10µm**	**>15µm**
Number of data points in the statistics	n	4623	2189
Exponent of the l-MSD power-law			
all	$<\alpha>$	1.64	1.45
dir-runs	$<\alpha_d>$	1.82	1.81
rm-modes	$<\alpha_r>$	1.26	1.31
Instantaneous velocity (µm/s)			
all	$<V>$	0.040	0.040
dir-runs	$<V_d>$	0.059	0.048
rm-modes	$<V_r>$	0.031	0.035
***dir*-runs lifetime (s)**	$<\tau_d>$	120	108
***dir*-run length (µm)**	$l_{d,\,cut}$	8.4	5.8

Table S1: Parameters describing the cell motility within micropillar networks of varying interpillar distance, corresponding to Fig. 3, Fig. S1 to S3.

B. Supplementary Text

Text S1. Details concerning cell motility behavior on flat PDMS

We studied the spontaneous migration of single cells (N = 27 cells, n = 10968 data points) on flat PDMS substrates by applying both a global analysis and the time-resolved TRAnSpORT algorithm. The characteristic features are illustrated in Fig. 2 and summarized in Table 1.

Global MSD analysis The global MSD functions, calculated over the entire trajectories, yield information about the cell migration type as a whole. A typical example function is given in Fig. 2N (corresponding track shown in insert). The motion is superdiffusive at short time scales (power-law trend exponent $\alpha_1 = 1.70 >> 1$) and diffusive at long time scales (power-law trend exponent $\alpha_2 = 1.09 \approx 1$), with a typical cross-over time from one regime to the other of $\tau_C = 256s$. The statistics on all cells yield average values of the same order: $\langle \alpha_1 \rangle = 1.54 \pm 0.18$, $\langle \alpha_2 \rangle = 1.11 \pm 0.31$ and $\langle \tau_C \rangle = 207 \pm 124s$. But this global analysis can only give a rough representation of cell migration as a random walk which, at short time scales, involves periods of rather directed migration. While the double fitting of the global MSD functions can only yield one characteristic cross-over time τ_C, our high resolution analysis of local motion types enables to separate the contributions of different migration modes, and to analyze the distribution of their precise characteristics: local MSD exponent, velocity and lifetime.

Local MSD analysis The α-landscape of local MSD functions (Fig. 2B) shows a succession of ballistic-like (local exponent of the power law, $\alpha \geq 1.65$) and diffusive-like ($\alpha \leq 1.35$) phases, with an overall tendency towards superdiffusion. By correlating the values of the local exponent α and angle persistency $\Delta\phi$ (see Materials and Methods), we were able to split the cell migration trajectories into two specific motility types: *dir* -runs, or phases of directed motion, which also exhibit high velocities ($\langle v_d = 0.076 \mu m \cdot s^{-1} \rangle$), separated by *rm*-modes, i.e. slower phases of random probing ($\langle v_r = 0.057 \mu m \cdot s^{-1} \rangle$).

The distribution of the local exponents α confirms the tendency of cells to move in a directed way: it peaks around 1.8 (Fig. 2F). A second small bump in the distribution can be seen for α_1, which corresponds to the *rm*-modes, during which the cell randomly probes its environment and has a diffusive-like trajectory.

Moreover, the angle distributions of both phases, whether on a short or a long time scale, exhibit no particular trend in direction. So, the symmetry breaking, that triggers each directed phase, is isotropic.

Text S2. Details concerning cell motility behaviour within regular and homogeneous micropillar arrays

To extract the effect of micron-scale topography on amoeboid motility, we placed the cells in dense, regular arrays of micropillars (Fig. 1E). In this case, the cells have to squeeze in between pillars to move.

We studied the characteristics of the two motility modes, i.e. directed runs and random probing (N = 13 cells, n = 5178 data points), and noticed very clear differences to the spontaneous motion on a 2D surface, as illustrated in Fig. 2 and Table 1. The fact that the flat reference and the microstructured substrates consist of the same material (PDMS) ensures that any difference in cell motility can only be attributed to the well-defined micron-scale topography, and not to different chemical properties of the surface.

Global MSD analysis As seen for the typical cell track analyzed on Fig. 2O, the global MSD function exhibits a trend towards subdiffusion at long time scales ($\alpha_2 = 0.77$). Even though the motion remains superdiffusive at short time scales, the exponent is lower than on flat ($\alpha_1 = 1.23$), and the cross-over time is shorter ($\tau_C = 188s$). So the cell overall migration is less effcient, and results in a more confined random walk. This is confirmed by average values: $\langle \alpha_1 \rangle = 1.31 \pm 0.14$, $\langle \alpha_2 \rangle = 0.87 \pm 0.32$ and $\langle \tau_C \rangle = 176 \pm 84s$. Also, the average cell velocity is lower than the reference velocity on flat: $\langle V \rangle_{pil} = 0.043 \mu m \cdot s^{-1}$ instead of $\langle V \rangle_{ref} = 0.057 \mu m \cdot s^{-1}$ (Fig. 2C).

Local MSD analysis After splitting into the two motility modes, we observe that the velocity of the *dir*-runs is larger $\langle V \rangle_{pil} = 0.082 \mu m \cdot s^{-1}$ instead of $\langle V \rangle_{ref} = 0.077 \mu m \cdot s^{-1}$ on flat. The *dir*-runs are much less frequent: within this very dense micropillar environment, they represent only 10% of the total time, as opposed to 35% for the spontaneous motility on a flat substrate. This tendency of cells to move in a more erratic way is reflected in the α exponent distribution (Fig. 2G): it is peaked around 1.5, significantly lower than the reference distribution. The *dir*–run lifetimes decay much faster: fitting by a simple exponential yields a characteristic time of $\langle \tau_d \rangle = 111s$.

Finally, the most striking trend can be seen in the angle distribution of *dir*–runs (Fig. 2C): in such a topographical environment, the directed modes of motion do not occur in random directions any more. They are guided along the main axes of the lattice. The random probing modes, however, remain randomly oriented. This already shows that topographical features act as a guide for cell migration only by directing the ballistic phases of motion.

Here, our observation of cell migration in two drastically different topographical situations gives hints about the way motion is affected by dense microstructures, but does not yield information about the transition from one topographical environment to the other.

To study the migration transition at the interface between flat and microstructured environments, we recorded Dd cell migration within scarcely distributed islands of micropillar arrays, separated by large areas of flat surface. In addition to the dynamical motility features, we observed the steady-state spatial distribution of cells in environments where different topographical environments are adjoining, evidencing trends in cell localization towards microstructures.

Text S3. Details concerning the motility behavior within low-density islands of micropillars

We analyzed cell migration (N = 27 cells, n = 10220 data points) in environments composed of low-density islands of micropillars (Fig. 1I, 3C). Out of the 27 cells, 14 (50%) were observed to be in contact with pillars for all or a fraction of their trajectory. Out of them, 9 (75% of the contacting cells) displayed losing and re-establishing contact with pillars several times[1].

3.1. Description of typical motion features

Typical trajectories observed for cells migrating at the interface between the 2D surface and the 3D micropillars are presented in Fig. S3A, C and E (and the corresponding movies S3, S5, and S4 respectively).

The slow and probing cells display "stick-and-go". When a cell reaches a pillar, it typically stays in contact with it for more than 200 s (Fig. S3A,E). Upon detaching from it, the cell starts crawling on the flat PDMS, and performs a sequence of short *dir*-/*rm*-phases, going back and forth for 200 to 500 s (Fig. S3B).

Within that searching time, a "stick-and-go" motion feature was observed for most cells (60% of the contacting cells) as a typical reaction to pillar contact: either the cell finds another pillar, which becomes the new starting point of the next "stick-and-go" series, or the cell finds its way back to the same pillar. In both cases, long interaction times between cell and pillar are observed.

The revisiting events, often displayed several times successively, are a very interesting feature. Indeed, one would not expect them in the frame of an optimized searching process, and show that the complex internal signalling cascades triggered by prolonged micropillar contact (over 500 s) result in cell relocalization towards topographical features. The fact that cells have a certain biochemical "memory" of the obstacles they were in contact with can however be linked to another motion feature: on flat substrates, motion of the cell along its own previous track can sometimes be observed (Fig. 1DA and movie S1), reflecting the cell sensing of its own left-over protein traces [*SR1*].

The fast and efficiently migrating cells are deflected by pillars. If no other pillar is present in the cell vicinity after 500 to 1000 s of probing, the cell repolarizes in a new direction and starts a new *dir*–run (Fig. S3C, D: orange arrows). A cell which is then in a fast *dir*-run displays a very different reaction to pillar contact: when touching a pillar, it is deflected by it, but does not show any slowing down nor does it stay in contact with the micropillar for more than 100 s (Fig. S3C-D: white arrow, and movie S5). On the flat part of the substrate, such cells are exhibiting very frequent and long *dir*-runs, with a speed higher than $0.1\mu m \cdot s^{-1}$, which is at the upper limit of the overall speed distribution, since 70% of the *dir*-run speed values on 2D substrates are between zero and $\langle V_d \rangle + 3\sigma_{Vd} = 0.093\mu m \cdot s^{-1}$ (Fig. 2B).

3.2. Statistical results

Partition coefficient between flat and microstructured substrates Once given the possibility to stay on the flat part of the substrate or to come in contact with micropillars, the cells tend to spend a very high fraction of their time in contact with pillars. The overall statistics yield a "relocalization" factor R of almost 3 (Fig. 3D). This factor is calculated as the ratio of two

[1] We also observed cells staying on top of a pillar and turning around it on its edge, which proves that *D. discoideum* cells are sensitive to the high curvature present at the border between pillar top and pillar walls. Such a case can be observed in movies S3 and S9.

dimensionless numbers:

$$R = \frac{T_{cont}/T_{tot}}{\sum_{pil}/\sum_{flat}}$$

The numerator, T_{cont}/T_{tot}, represents the fraction of the time the cells spend in contact with pillars, for all measured cells: T_{cont} takes into account all the time points for which the contact index is greater than 1 and T_{tot} is the total number of time points recorded. The denominator, $\sum_{pil}/\sum_{flat}$ represents the fraction of the surface available for cells in the neighbourhood of pillars, as measured on the images. So the fact that we obtain a factor $R = 2.75$ means that the cells tend to stay almost three times longer in contact with pillars than on flat.

If we take into account the additional surface offered by pillar walls in the vertical direction, we retrieve a surface ratio $\sum_{pil}/\sum_{flat}$ twice larger. It results in a new ratio $R_{addsurf} \cong 1$. So, by taking into account the additional surface offered to the cells by the pillar walls, we obtain an equal distribution between cells on flat and cells in contact with microstructures.

This relocalization factor can also be seen as a steady-state partition coefficient: when considering the dynamical behavior of cells at the transition between a flat and a microstructured landscape, this coefficient represents the trend for cells to remain in one or the other topographical environment. We show here that the observed partition can be explained exclusively by an additional surface effect.

Cell attraction to micropillars as a dynamical effect The velocity distributions obtained from the time points during which the cells touch 1 or 2 pillars are slightly shifted towards smaller values, compared to the reference velocity distribution for cells migrating on flat PDMS (Fig. 3E). Indeed, the velocity distributions peak around $0.03\mu m \cdot s^{-1}$ for the flat case, $0.02\mu m \cdot s^{-1}$ for $I_{cont} = 1$ and $0.01\mu m \cdot s^{-1}$ for $I_{cont} = 2$. However, this shift is small compared to the standard deviation of the distributions (around $0.04\mu m \cdot s^{-1}$ in all three cases), and the median velocity stays within 10% around the value of $0.05\mu m \cdot s^{-1}$, as shown in insert of Fig. 3E.

In summary, the observed cell motion while in contact with a micropillar results from the superposition of the following counter-acting effects:

(1) an "additionally available surface" effect: the probability that random protrusions touch a surface is increased. If a pseudopod establishes contact with the micropillar surface, feedback loops are activated locally and trigger actin polymerization which stabilizes the pseudopod. The resulting probability that this pseudopod becomes a leading one, and hence the probability that a *dir*-run starts, is increased.

(2) a "three-dimensional motion" effect: when a *dir*-run starts upon micropillar contact, the cell moves partially in the *Z*-direction, but the *Z*-component of the velocity cannot be measured by our standard epifluorescence observations. Hence, the measured velocity is lower than the actual one and the proportion of *dir*-runs retrieved by analysis is also biased towards lower values, due to the undetected motion in the *Z*-direction.

The first effect tends to increase the proportion of directed motion modes, while the second tends to decrease it. As a result, a very slight decrease can be observed both in the velocity, as described above, and in the *dir*-run frequency upon pillar contact: from 35% on flat to 27% when touching two pillars (Fig. 3F).

This amoeboid search mechanism and its modification upon topography sensing appears strikingly similar to the one described for bacterial chemotaxis: the run-and-tumble mechanism and its modification upon gradient sensing have long been shown [*SR3, SR4*]. The underlying theory is that the spontaneous motion consists of a superposition of two states, each being a random walk on a different length scale (the directed runs result in long-distance bacteria motion while the tumble modes allow for local probing), and that chemotaxis results from a shift in the distribution of the state frequency. But in the case of bacteria, due to their small size, the long and directed runs remain randomly oriented, and the cell motion up-gradient only results from a

switch in frequency. While here, the orientation of the *dir*-runs is biased by topography sensing, because contact of one cell protrusion with a surface polarizes the cell into a new preferred direction.

3.4 Cell interaction with individual micropillars

Within the framework of our two-state model, we investigated interaction types of single cells with individual micropillars. As elaborated above for cell behavior on flat substrates, we observed the following characteristics:

(i) for cells which are initially in the random probing *rm*-mode: they frequently return to pillars after first pillar contact (Fig. S3A-B, S3C-D and movies S3 and S4). This revisiting effect can occur several times successively, which is not expected in the framework of an optimized search process. This proves that a cell in the probing *rm*-mode will be very sensitive to the positive feedback provided by contact with a pillar: the pillar walls offer additional surface in the third dimension (see scheme in Fig. 3B) and as a consequence, the probability for a randomly extruded cell protrusion to become the leading pseudopod is increased by pillar contact. The new direction of the cell motion is hence biased towards the pillar and the cell seems to be trapped around it.

(ii) for cells which are initially in a fast *dir*-run: upon touching a pillar, their *dir*-run is deflected. They slightly slow down and repolarize into a new direction after pillar contact. They rarely stay in contact with the micropillar for more than 100 s (Fig. S3E-F and movie S5) and do not remain trapped around it.

Micropillars as an indicator of the cell migration type

These two drastically different ways of reacting to micron-scale topography allow us to easily distinguish between two extreme types of motility states, while the cell-to-cell variability observed on a flat substrate is harder to categorize. Indeed, on flat substrates, the run-and-search motility includes all cell behaviors, ranging from the slow and probing cells to the fast and efficient cells. However, when in contact with a microstructure, cells in the *rm*-mode appear to be very sensitive to topographical cues and stay in contact with them for very long periods (over 500 s), tending to return when they do not find another pillar close-by. Conversely, the fast and efficient *dir*-run cells merely sense the topography and react to it with no other trajectory modification than a deflection.

Also, since cells can switch from one migration type to the other (as evidenced in Fig. S3C and movie S5), the presence of a topographical feature in the cell neighbourhood allows for the rapid discrimination between one or the other cell behavior type. Interestingly, the fact that a cell hits the pillar head-on or sideways is not decisive for the type of reaction triggered (see Movies S3 and S5: two cells hit a pillar sideways, but for one cell this results in a prolonged contact (S3), whereas it leads to deflection for the other cell (S5)).

C. Supplementary References

SR1. M. Schindl, et al., *Biophys*. J., 1995,**68**, 1177.
SR2. T. Bretschneider, et al., *Biophys. J.*, 2009, **96**, 2888.
SR3. H. Berg and D. Brown, *Nature*, 1972, **239**, 500.
SR4. J. Adler, *Science,* 1969, **166**, 1588 .

D. Description of the supporting movies

Movie S1 *D. discoideum* cell migrating freely on a flat PDMS substrate.
Corresponding trajectory : Fig. 1D.

Movie S2 *D. discoideum* cell migrating within a dense rectangular array of PDMS micropollars. In order to be easily followed over the movie, the cell is highlighted by a white circle.
Corresponding trajectory: Fig. 1E.

Movie S3 *D. discoideum* cell migrating at the frontier between micropillars and the flat substrate. The cell displays revisiting "stick-and-go", by coming back twice to the same pillar.
Corresponding trajectory: Fig. S3A.

Movie S4 *D. discoideum* cell migrating at the frontier between an island of micropillars and the flat substrate. The cell displays "stick-and-go", by going from pillar to pillar.
Corresponding trajectory: Fig. S3C.

Movie S5 *D. discoideum* cell migrating at the frontier between an island of micropillars and the flat substrate. The cell switches from slow (pillar-sensitive) motility at the beginning to fast and efficient (pillar-insensitive) migration at the end (where pillar contact only results in the deflection of the cell). The switching time at which the cell repolarizes and starts migrating fast into a new direction is indicated by a red circle.
Corresponding trajectory: Fig. S3E.
(N.B. : movie has been rotated by 90 deg. with regard to the original images, for file compressing reasons)

Movie S6 *D. discoideum* cell migrating within a micropillar array of low density, going from pillar to pillar. The cell of interest is highlighted by a white circle at the beginning of the movie.
Corresponding trajectory: Fig. S1A.

Movie S7 *D. discoideum* cell migrating within a micropillar array of low density, going from pillar to pillar and covering a very long distance.
Corresponding trajectory: Fig. S1B.
(N.B. : movie has been rotated by 90 deg. with regard to the original images, for file compressing reasons)

Movie S8 *D. discoideum* cells migrating within a micropillar array of intermediate density, at which they can touch two pillars at the same time. The cells then display stalling behavior, highlighted by magenta circles.
Corresponding trajectory: Fig. S2D.